Structure of ${}^{9}_{\Lambda}$Be and ${}^{10}_{\Lambda\Lambda}$Be using the beyond-mean-field Skyrme-Hartree-Fock approach

Wen-Ying Li,[1] Ji-Wei Cui,[2,*] and Xian-Rong Zhou[1,†]

[1]*Department of Physics, East China Normal University, Shanghai 200241, People's Republic of China*

[2]*School of Physics and Optoelectronic Engineering, Xidian University, Xi'an 710071, People's Republic of China*

(Received 19 September 2017; published 2 March 2018)

Based on the beyond-mean-field Skyrme-Hartree-Fock model, the up-to-date Skyrme-type $N\Lambda$ interaction, SLL4, is used to investigate the properties of ${}^{9}_{\Lambda}$Be comprehensively. Energies of different configurations, such as ${}^{8}\mathrm{Be}\otimes\Lambda[000]1/2^{+}$, ${}^{8}\mathrm{Be}\otimes\Lambda[110]1/2^{-}$, ${}^{8}\mathrm{Be}\otimes\Lambda[101]3/2^{-}$, and ${}^{8}\mathrm{Be}\otimes\Lambda[101]1/2^{-}$ are given and used to study the effects of Λ occupying different orbitals. The calculated energy spectra, including both positive- and negative-parity levels, are given and compared to the experimental data. The observed positive-parity spin doublets $(3/2^{+},5/2^{+})$ are successfully reproduced, but the energy difference needs further investigation. The two well-known band structures corresponding to the genuine hypernuclear states and the ^{9}Be-analog states are also obtained and compared with the observed ones. The shrinkage effect of Λ occupying $\Lambda[000]1/2^{+}$ is investigated through the density distributions of nuclear core. And finally, the $E2$ transition rates are given and compared with the observed data and with the results of the hypernuclear particle-rotor model. Properties of ${}^{10}_{\Lambda\Lambda}$Be are also studied to show the completeness of this current model.

DOI: 10.1103/PhysRevC.97.034302

I. INTRODUCTION

In the past several decades, progress of hypernuclear experiments has provided fruitful data for better understanding the structure of Λ hypernuclei and investigating the $N\Lambda$ interaction [1–4]. Among lots of observed Λ hypernuclear systems, ${}^{9}_{\Lambda}$Be is a a good example, characterized by a three-body structure $(\alpha\alpha\Lambda)$, and different positions of Λ with respect to the nuclear core $(\alpha\alpha)$ lead to different band structures, which are typically observed and studied in detail [5–14]. It is worth mentioning that in Ref. [7] a fully microscopic cluster model calculation was applied to ${}^{9}_{\Lambda}$Be, and then a comprehensive investigation was made for several p-shell hypernuclear systems including ${}^{6}_{\Lambda}$He, ${}^{6-8}_{\Lambda}$Li, and ${}^{8-9}_{\Lambda}$Be in a unified way [8,9]. For ${}^{9}_{\Lambda}$Be, the Be-analog state (with a Λ hyperon moving parallel to the α-α deformation axis) and genuine hypernucler state (with a Λ hyperon moving in the plane perpendicular to the α-α deformation axis) were first pointed out by the authors of Refs. [7–9]. For ${}^{10}_{\Lambda\Lambda}$Be, there is an observed energy level which is believed to be the first 2^{+} state [15], and the energy of ground state is estimated by different theories [16,17].

Besides the shell models [17–20] in the early years and the microscopic cluster model calculations [7–12,16,21–24] mentioned above, there are several other nuclear models which are extended to the hypernuclear sector, such as the self-consistent mean-field models [25–38], asymmetrized molecular dynamics (AMD) [39–43] and *ab initio* calculations [44]. Self-consistent mean-field models based on energy density functional (EDF) theories, namely the Skyrme-Hartree-Fock (SHF) model and relativistic mean-field (RMF) model, seem to be the only kind which are not hindered by the increasing mass number of the nuclear core and thus can give global investigations across the hypernuclear chart. The up-to-date Skyrme-type $N\Lambda$ interaction, SLL4, is the stateof the art of its kind and gives a very good fitting for the Λ binding energies in a wide range of hypernuclear mass numbers [45].

However, there are two major shortcomings for such mean-field calculations. The first one is the broken rotational symmetry built in the mean-field models, which make it difficult to give the low-lying energy spectra. The second one is the fact that the mean-field models rely on a single configuration, which would leads to bad predictions. For example, using the SLL4 parameter set, the calculation with the spherical configuration predicts B_{Λ} of ${}^{9}_{\Lambda}$Be as 8.02 MeV, which is 1.3 MeV higher than the observed one, since the two-α cluster structure of the nuclear core, ^{8}Be, is missed in the configuration employed [45]. To overcome these two drawbacks, the beyond-mean-field calculation is extended to the hypernuclear regime for both the RMF [46,47] and SHF [48,49] models and give successful predictions for ${}^{13}_{\Lambda}$C and ${}^{21}_{\Lambda}$Ne. In those calculations, angular momentum projection (AMP) is used to restore the rotational symmetry and generator coordinate method (GCM) is employed to mix configurations from different mean fields. Compared to the other analogs [50–54], the advantage of the hypernuclear beyond-mean-field calculations is the fact that they treat both the nucleons and hyperons on the same footing.

In this paper, the beyond-mean-field SHF method is implemented to study ${}^{9}_{\Lambda}$Be for two aims. The first one is to give a more detailed and comprehensive investigation about the three band structures mentioned at the beginning. The second one is to test the validity of the Skyrme-type $N\Lambda$ interaction, SLL4, in the three-body structure, $\alpha\alpha\Lambda$. And for completeness of the

*jwcui@xidian.edu.cn

†xrzhou@phy.ecnu.edu.cn

model, ${}^{10}_{\Lambda\Lambda}$Be with the configuration $[(\alpha\alpha)\otimes s^2_\Lambda]_{K=0^+}$ is also investigated as a supplement.

This paper is organized as follows. In Sec. II, formalism of the beyond-mean-field calculation is introduced. Section III presents the results and discussions. In Sec. IV, we draw conclusions about the paper.

II. FORMALISM

We start from the EDF of the (double-)Λ hypernuclear mean field,

$$\epsilon = \epsilon_N^{\text{Skyrme}} + \epsilon_\Lambda \,, \tag{1}$$

where $\epsilon_N^{\text{Skyrme}}$ is a Skyrme-type EDF for the nuclear core and ϵ_Λ accounts for the energy due to the addition of one or two Λ hyperons. It is divided into three parts as

$$\epsilon_\Lambda = \frac{\hbar^2}{2m_\Lambda}\tau_\Lambda + \epsilon_{N\Lambda} + \epsilon^\Lambda_{\text{s.o.}} \,, \tag{2}$$

where $\epsilon_{N\Lambda}$ represents a nonrelativistic $N\Lambda$ interaction without the spin-orbit part in Ref. [45], and the spin-orbit part $\epsilon^\Lambda_{\text{s.o.}}$ is included in this current work as [30]

$$\epsilon^\Lambda_{\text{s.o.}} = -\tfrac{1}{2}W_\Lambda(\rho_\Lambda\nabla\cdot J_N + \rho_N\nabla\cdot J_\Lambda)\,. \tag{3}$$

In a body-fixed frame of reference, the wave function of a (double-)Λ hypernuclear system takes the form of

$$|\Phi^{(N\Lambda)}(\beta)\rangle = |\Phi^N(\beta)\rangle\otimes|\Phi^\Lambda\rangle \,, \tag{4}$$

where $|\Phi^N(\beta)\rangle$ is the wave function for the nuclear core with quadrupole deformation β and $|\Phi^\Lambda\rangle$ for the Λ hyperons, respectively. In hypernuclear SHF model, the intrinsic wave function $|\Phi^{(N\Lambda)}(\beta)\rangle$ is derived by the variation of Eq. (1) with the help of a constraint on quadrupole moment, ensuring that the whole system is axially symmetrized with respect to the body-fixed z axis.

It is worth mentioning here that the paring force of the nuclear core takes the form of a density-dependent δ interaction (DDDI) [55] as follows:

$$G(\mathbf{r}) = V_0\left[1 - \frac{\rho(\mathbf{r})}{\rho_0}\right], \tag{5}$$

where the saturation density ρ_0 equals 0.16 fm^{-3}.

In a way similar to Ref. [37] and with some little changes, single-particle orbitals of the Λ hyperon are labeled by the Nilsson quantum numbers $\Lambda[Nn_3m_l]K^\pi$, and only four orbitals are, respectively, taken into consideration for s_Λ and p_Λ shells as $\Lambda[000]1/2^+$, $\Lambda[110]1/2^-$, $\Lambda[101]3/2^-$, and $\Lambda[101]1/2^-$. So, in this current paper, the configuration of a single-Λ hypernuclear system ${}^9_\Lambda$Be is denoted by ${}^8\text{Be}\otimes\Lambda[Nn_3m_l]K^\pi$. References [2,12] adopt the notation such as $[(\alpha\alpha)\otimes p^\parallel_\Lambda]_{K=0^-}$, where K means the third component of the orbital angular momentum, but in this paper, K denotes the third component of total spin.

For the double-Λ hypernuclei, ${}^{10}_{\Lambda\Lambda}$Be, since the current work just focuses on the configuration where the two Λ hyperons occupy the s_Λ orbital, the wave function of hyperonic part takes the antisymmetrized form

$$|\Phi^\Lambda\rangle = \frac{1}{\sqrt{2}}\left[\varphi^\Lambda_s(\Lambda_1)\varphi^\Lambda_{\bar{s}}(\Lambda_2) - \varphi^\Lambda_s(\Lambda_2)\varphi^\Lambda_{\bar{s}}(\Lambda_1)\right], \tag{6}$$

where φ^Λ_s and $\varphi^\Lambda_{\bar{s}}$ are time-reversal partners of the s_Λ orbital.

To restore the rotational symmetry of $|\Phi^{(N\Lambda)}(\beta)\rangle$ and to take the dynamical correction into consideration, the eigenstate of a hypernuclear system is given as a superposition,

$$\left|\Psi^{JM}_\alpha\right\rangle = \sum_\beta F^J_\alpha(\beta)\hat{P}^J_{MK}|\Phi^{(N\Lambda)}(\beta)\rangle \,, \tag{7}$$

where $\hat{P}^J_{MK}$ is the AMP operator. K is the projection of the total angular momentum on the z axis of the body-fixed frame of reference, and it is divided into two parts for the nuclear core and hyperons, respectively,

$$K = K_c + K_\Lambda. \tag{8}$$

Because of the time-reversal symmetry for the nuclear core, K_c equals zero and thus K equals to K_Λ.

Before going further, it must be emphasized that the three negative-parity configurations mentioned above would mix each other to some extent via the $N\Lambda$ interaction. In this paper, such mixing is not taken into consideration, which implies that there is no K mixing in the eigenstate $|\Psi^{JM}_\alpha\rangle$.

In Eq. (7), the eigenstates $F^J_\alpha(\beta)$ are determined by the Hill-Wheeler-Griffin (HWG) equation [56],

$$\sum_{\beta'}\left[H'^J_{KK}(\beta,\beta') - E^J_\alpha N^J_{KK}(\beta,\beta')\right]F^J_\alpha(\beta') = 0 \,, \tag{9}$$

where the Hamiltonian and norm elements are given by

$$H'^J_{KK}(\beta,\beta') = \langle\Phi^{(N\Lambda)}(\beta')|\hat{H}'\hat{P}^J_{KK}|\Phi^{(N\Lambda)}(\beta)\rangle, \tag{10}$$

$$N^J_{KK}(\beta,\beta') = \langle\Phi^{(N\Lambda)}(\beta')|\hat{P}^J_{KK}|\Phi^{(N\Lambda)}(\beta)\rangle. \tag{11}$$

The corrected Hamiltonian $\hat{H}'$ is

$$\hat{H}' = \hat{H} - \lambda_p(\hat{N}_p - Z) - \lambda_n(\hat{N}_n - N) \,, \tag{12}$$

where the last two terms on the right-hand side account for particle-number correction since the AMP operator makes the average particle number deviate from the real one [57–59], and $\hat{H}$ is determined by the EDF in Eq. (1).

Given that the eigenstates are determined, the reduced $E2$ transition rates are derived as

$$B(E2, J\alpha\to J'\alpha') = \frac{1}{2J+1}|\langle\alpha';J'||\hat{Q}_2||\alpha;J\rangle|^2 \,, \tag{13}$$

where

$$\langle\alpha';J'||\hat{Q}_2||\alpha;J\rangle = \sqrt{2J'+1}\sum_{M\mu\beta\beta'}F^{J'*}_{\alpha'}(\beta')F^J_\alpha(\beta)C^{J'K'}_{JM2\mu} \times\langle\Phi^{(N\Lambda)}(\beta')|\hat{Q}_{2\mu}\hat{P}^J_{MK}|\Phi^{(N\Lambda)}(\beta)\rangle \,, \tag{14}$$

in which $\hat{Q}_{2\mu} = r^2Y_{2\mu}(\varphi,\theta)$ is the electric quadrupole transition operator and $C^{J'K'}_{JM2\mu}$ denotes the Clebsh-Gordon coefficients [60].

A. Parameters

In this current paper, SLy4 force is used for the NN interaction and the strength of the pairing force is $V_0 = -410$ MeV fm^3 for both protons and neutrons [61] with a smooth pairing

energy cutoff of 5 MeV around the Fermi level [30,62,63]. For $N\Lambda$ interaction, SLL4 force [45] is used and the strength of hyperonic spin-orbit force is adjusted to $W_\Lambda = 5.0$ MeV fm^5 which can reproduce the observed spin-orbit splitting [64] through mean-field calculation with a spherical configuration [49].

B. Model space

Because the intrinsic wave functions are kept axially symmetric, the range of β and the number of basis functions determine the model space. In this current calculation, for ^{8}Be, ${}^{9}_{\Lambda}$Be, and ${}^{10}_{\Lambda\Lambda}$Be, β is from -3.6 to 8.5, and 86 basis functions are evenly spaced in this range. Actually, the weights of the basis functions out of the range -3.0 to 7.0 are more than two orders smaller than the weight of the most important one and play negligible roles. For the low-lying energy levels, increasing number of basis functions within the chosen range makes nearly no differences.

III. RESULTS AND DISCUSSIONS

In this section, the model introduced above is applied to ^{8}Be, ${}^{9}_{\Lambda}$Be, and ${}^{10}_{\Lambda\Lambda}$Be, respectively. The potential energy surfaces (PESs), (double-)Λ binding energies, (hyper)nuclear density distributions, band structures, and $E2$ transitions are discussed in detail.

Figure 1 gives the PESs of different configurations obtained from SHF mean-field calculations. It is shown that the energy curve of ^{8}Be has a minimum on the prolate side with $\beta = 1.1$, which indicates a superdeformed shape. Because of the well-known shrinkage effect, the addition of Λ to the lowest orbital $\Lambda[000]1/2^+$ makes the energy minimum of ${}^{9}_{\Lambda}$Be slightly closer to the spherical shape, i.e., $\beta = 1.0$. The configuration ${}^{8}\text{Be} \otimes \Lambda[110]1/2^-$ leads to a more obvious energy minimum on the prolate side, while the configurations ${}^{8}\text{Be} \otimes \Lambda[101]3/2^-$ and ${}^{8}\text{Be} \otimes \Lambda[101]1/2^-$ give nearly identical oblate energy minima. Different effects of three p_Λ orbitals on the energy curves origin from their different density distributions, or rather, $\Lambda[110]1/2^-$ is prolately distributed while $\Lambda[101]3/2^-$ and $\Lambda[101]1/2^-$ are oblate ones. The spin-orbit splitting is obviously shown in the inserted graph of Fig. 1 and the energy difference between the configurations $[{}^{8}\text{Be} \otimes (p_{1/2})_\Lambda]$ and $[{}^{8}\text{Be} \otimes (p_{3/2})_\Lambda]$ is 149 KeV. Also in the inserted graph, the no-crossing rule is reproduced (for more details about no crossing rule, please refer to pages 76–77 of Ref. [56], or pages 259–260 of Ref. [65]), which makes the energy curves of ${}^{8}\text{Be} \otimes \Lambda[110]1/2^-$ and ${}^{8}\text{Be} \otimes \Lambda[101]1/2^-$ noncontinuous at $\beta = 0$. This no-crossing phenomenon is caused by the addition of hyperonic spin-orbit term given in Eq. (3).

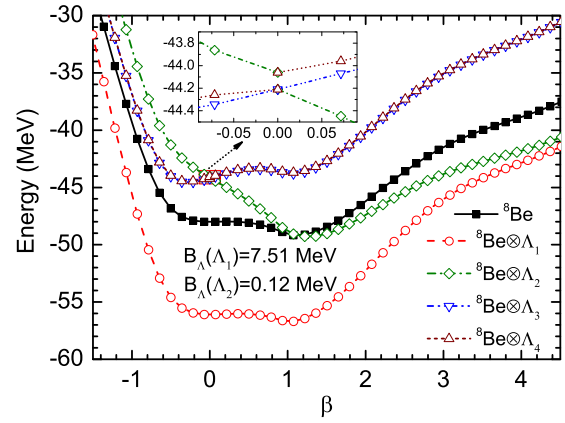

FIG. 1. PESs obtained from the mean-field calculations with different configurations. The inserted graph shows the spin-orbit splitting near the spherical shape, and Λ_1, Λ_2, Λ_3, and Λ_4 represent the single-Λ orbitals $\Lambda[000]1/2^+$, $\Lambda[110]1/2^-$, $\Lambda[101]3/2^-$, and $\Lambda[101]1/2^-$, respectively.

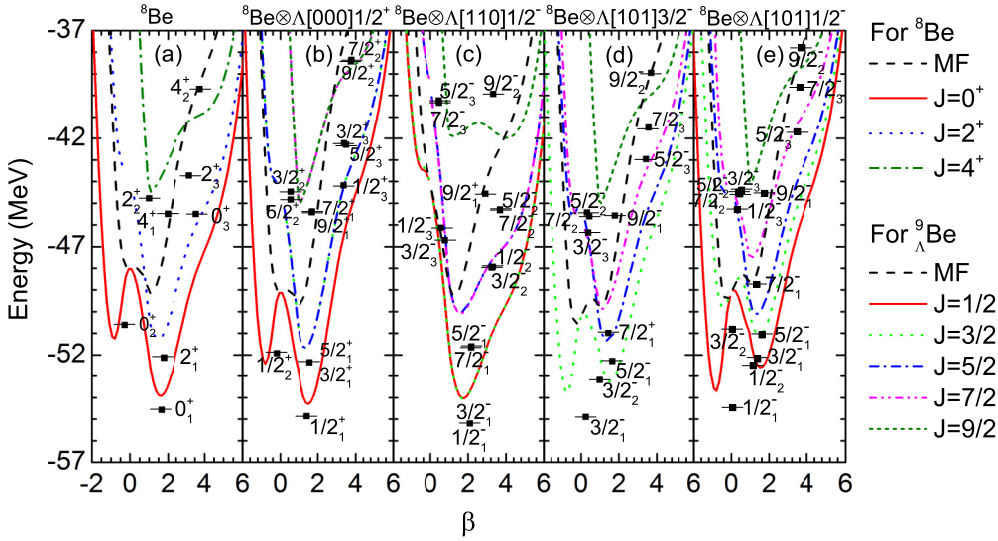

FIG. 2. Angular momentum projected energy curves for ^{8}Be and ${}^{9}_{\Lambda}$Be. Panel (a) is for ^{8}Be while panels (b), (c), (d), and (e) are for ${}^{9}_{\Lambda}$Be corresponding to the configurations ${}^{8}\text{Be} \otimes \Lambda[000]1/2^+$, ${}^{8}\text{Be} \otimes \Lambda[110]1/2^-$, ${}^{8}\text{Be} \otimes \Lambda[101]3/2^-$, and ${}^{8}\text{Be} \otimes \Lambda[101]1/2^-$, respectively. Some low-lying GCM levels are shown at average deformations $\bar{\beta}$. For the convenience of comparison, panels (b), (c), (d), and (e) are offset upward by 7, 0, -6, and -5 MeV, respectively.

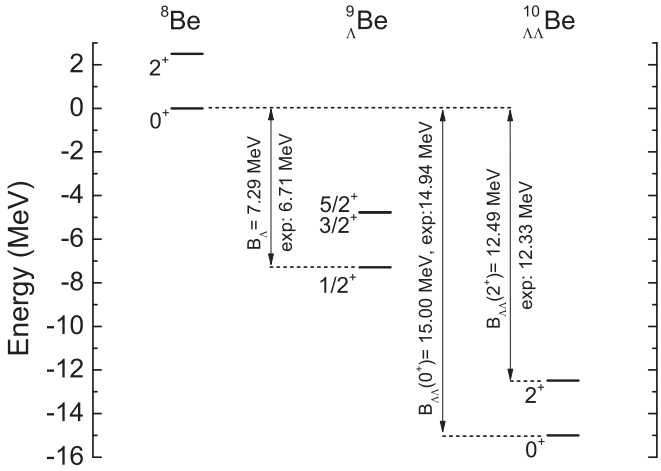

FIG. 3. The calculated positive-parity energy levels for ^{8}Be, $^{9}_{\Lambda}$Be, and $^{10}_{\Lambda\Lambda}$Be with respect to the ^{8}Be+$\Lambda(+\Lambda)$ threshold. The experimental data of ^{8}Be are from Ref. [66] and the observed (double-)Λ binding energies are from Refs. [17,67].

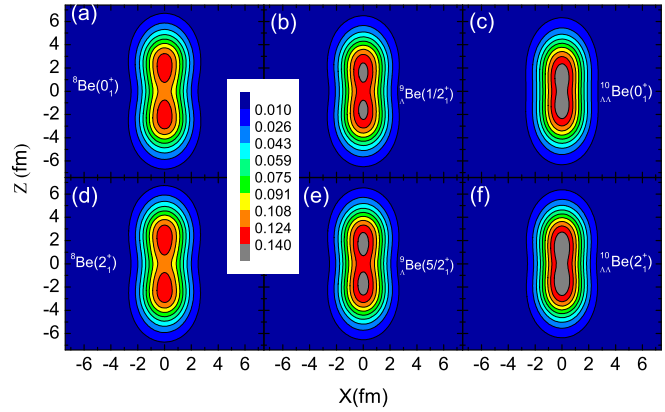

FIG. 4. Density distribution of nuclear matter for the 0^{+}_{1} and 2^{+}_{1} states of ^{8}Be [panels (a) and (d)] and $^{10}_{\Lambda\Lambda}$Be [panels (c) and (f)], and for the $1/2^{+}_{1}$ and $5/2^{+}_{1}$ states of $^{9}_{\Lambda}$Be [panels (b) and (e)] with configuration $^{8}\text{Be}\otimes\Lambda[000]1/2^{+}$. The six figures share the same color bar. The unit is set as fm^{-3}.

Figure 2 shows the AMP energy curves of different configurations. In Fig. 2(a), it is shown that the energies gained by AMP for the $J^{\pi}=0^{+}$ curve of ^{8}Be lead to two minima on the prolate and oblate sides, respectively. For the configuration $^{8}\text{Be}\otimes\Lambda[000]1/2^{+}$, in Fig. 2(b), we notice that the curves are similar to those of Fig. 2(a) but a little stiffer, which is caused by the impurity effect of Λ. For $^{8}\text{Be}\otimes\Lambda[110]1/2^{-}$ in Fig. 2(c), the oblate minima are eliminated, while for $^{8}\text{Be}\otimes\Lambda[101]3/2^{-}$ and $^{8}\text{Be}\otimes\Lambda[101]1/2^{-}$ in Figs. 2(d) and 2(e), respectively, the oblate minima are enhanced. The tendencies for different configurations originate from their density distributions, discussed above. The GCM calculations give some low-lying energy levels at $\bar{\beta}$ which indicate the average shapes of nuclear cores. It is shown that the ground state of ^{8}Be is at $\bar{\beta}=1.67$ in Fig. 2(a), and the shrinkage effect of Λ occupying the s_{Λ} orbital makes $\bar{\beta}$ reduced to 1.41 in Fig. 2(b). In the band-head state of the configuration $^{8}\text{Be}\otimes\Lambda[110]1/2^{-}$, $\bar{\beta}$ is increased to 2.1, since this configuration is an equivalent to $[(\alpha\alpha)\otimes p^{\parallel}_{\Lambda}]_{K=0^{-}}$ and the α-α structure is stretched along the symmetry axis by the Λ occupying the orbital $\Lambda[110]1/2^{-}$. While for $^{8}\text{Be}\otimes\Lambda[101]3/2^{-}$ and $^{8}\text{Be}\otimes\Lambda[101]1/2^{-}$ corresponding to $[(\alpha\alpha)\otimes p^{\perp}_{\Lambda}]_{K=1^{-}}$, the α-α structure is compressed dramatically as shown in Figs. 2(d) and 2(e) [in Figs. 2(d) and 2(e), $\bar{\beta}$ equals to 0.25 and 0.05, for the band-head states with $J^{\pi}=3/2^{-}$ and $J^{\pi}=1/2^{-}$ respectively].

In Fig. 3, the ground bands of ^{8}Be, $^{9}_{\Lambda}$Be, and $^{10}_{\Lambda\Lambda}$Be, with respect to the ^{8}Be+$\Lambda(+\Lambda)$ threshold, are given. It is shown that $B_{\Lambda}=7.29$ MeV, which is a little smaller than the one obtained from the deformed SHF calculation (7.51 MeV shown in Fig. 1). In Ref. [45], the SHF calculation with a spherical configuration gives $B_{\Lambda}=8.02$ MeV, which is obviously larger than the observed data (6.71 ± 0.04 MeV [67]) and it concludes that the spherical configuration used in the calculation leads to this problem, because it cannot give cluster structure of the core nucleus. In the current work, the inclusion of superdeformed configurations in the model space indeed reduces the Λ binding energy by about 0.8 MeV. Figures 4(a) and 4(b) show that the superdeformation, to some extent, gives a two-cluster structure. It is worth mentioning that the standard microscopic cluster model calculation [16], using preformed $\alpha\alpha\Lambda$ structure, gives B_{Λ} as 6.73 MeV, which is very close to the observed data.

In the current paper, we also calculate the energies of 0^{+}_{1} state and 2^{+}_{1} state of $^{10}_{\Lambda\Lambda}$Be with two Λ hyperons occupying the orbital $\Lambda[000]1/2^{+}$ and its time-reversal partner. In Fig. 3, it is shown that the calculated double-Λ binding energies of these two states are 15.00 and 12.49 MeV compared to the observed ones, 14.94 [17] and 12.33 MeV [15], respectively. However, the SLL4 froce in this current calculation does not include the $\Lambda\Lambda$ interaction, and if the calculated $B_{\Lambda\Lambda}$ is corrected by adding an attractive $\Lambda\Lambda$ interaction, i.e., $\langle V_{\Lambda\Lambda}\rangle>0$ [17], then it will be obviously larger than the observed data.

Figure 4 shows the shrinkage effects of the Λ hyperons occupying s_{Λ} orbital through the density distributions of the nuclear matter. In Figs. 4(a) and 4(d), we can see that the superdeformation makes the nuclear matter concentrate around two separated centers for both 0^{+}_{1} and 2^{+}_{1} states of ^{8}Be; and Figs. 4(b) and 4(e) show that the addition of one single Λ to $\Lambda[000]1/2^{+}$ makes the nuclear matter more concentrated on the original point. Furthermore, for $^{10}_{\Lambda\Lambda}$Be, Figs. 4(c) and 4(f) indicate that two Λ hyperons occupying the s_{Λ} orbitals make such a two-center structure disappear.

More comprehensive energy spectra of ^{8}Be and $^{9}_{\Lambda}$Be are shown in Fig. 5 and compared with the observed data. Besides the positive-parity energy levels with configuration $^{8}\text{Be}\otimes\Lambda[000]1/2^{+}$, three negative-parity bands with configurations $^{8}\text{Be}\otimes\Lambda[110]1/2^{-}$, $^{8}\text{Be}\otimes\Lambda[101]3/2^{-}$, and $^{8}\text{Be}\otimes\Lambda[101]1/2^{-}$ are also given, respectively. The spin doublet $(3/2^{+},5/2^{+})$ are reproduced at about 2.5 MeV compared to the observed one at 3.0 MeV. But the spin splitting in the current calculation is nearly zero compared to the observed one, 33 KeV [68], which is caused by the fact that the spin-spin interaction is not taken into account in the current SLL4 parameter. The two lowest negative-parity spin doublets $(3/2^{-},1/2^{-})$ and $(7/2^{-},5/2^{-})$, with configuration $^{8}\text{Be}\otimes\Lambda[110]1/2^{-}$, lo-

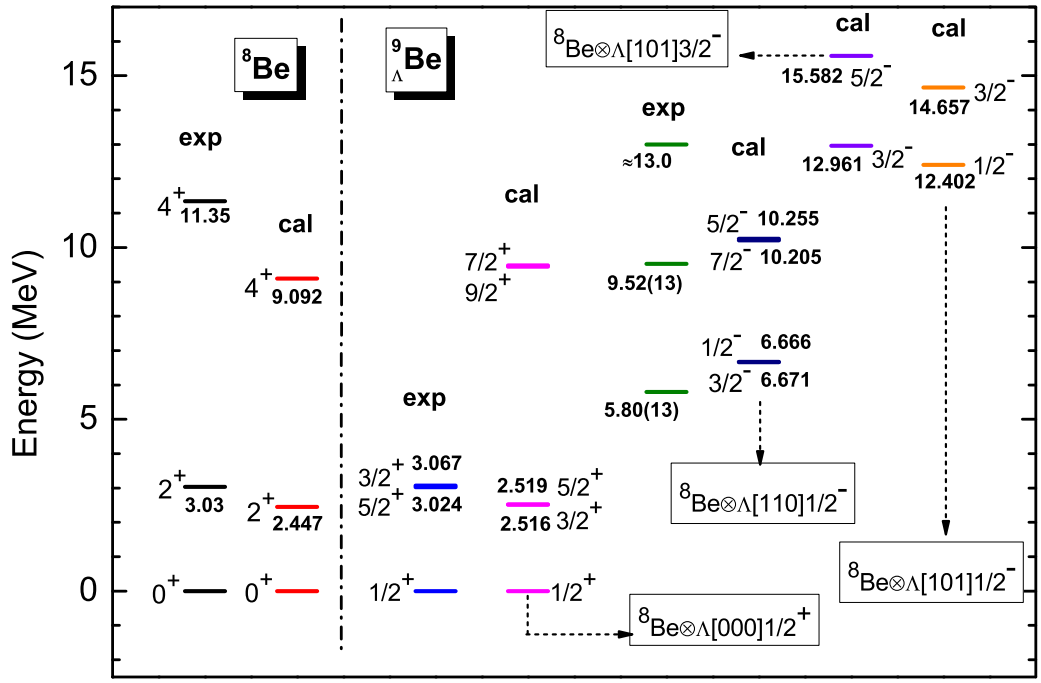

FIG. 5. Energy spectra of ^{8}Be, and of $^{9}_{\Lambda}$Be with configurations $^{8}\text{Be} \otimes \Lambda[000]1/2^+$, $^{8}\text{Be} \otimes \Lambda[110]1/2^-$, $^{8}\text{Be} \otimes \Lambda[101]3/2^-$, and $^{8}\text{Be} \otimes \Lambda[101]1/2^-$, respectively. The observed data of ^{8}Be are from Ref. [66] and those of $^{9}_{\Lambda}$Be are from Ref. [2,5,14,68,69].

cate at 6.7 and 10.2 MeV, which may be associated to the observed data, 5.80(13) and 9.52(13) MeV [2]. Namely, the configuration $^{8}\text{Be} \otimes \Lambda[110]1/2^-$ can successfully reproduce the genuine hypernuclear states. The $^{8}\text{Be} \otimes \Lambda[101]3/2^-$ and $^{8}\text{Be} \otimes \Lambda[101]1/2^-$ give energy levels several MeVs higher, with the band heads at 12.96 and 12.40 MeV, respectively. This is consistent with the second peak of the ^{9}Be (K^- in-flight, π^-) reaction [5] (in Ref. [5], the second peak is given at 6.3 MeV, which is 13.0 MeV higher than the ground state, i.e., the first peak at −6.7 MeV), and some models predict this peak as a ^{9}Be-analog state [12]. So the current model can give both the genuine hypernuclear states and the ^{9}Be-analog states.

To show the position of Λ with respect of the nuclear core more clearly, Fig. 6 gives the distributions of Λ for the bandhead states corresponding to the relevant four configurations. In Fig. 6(a), the density of Λ in the ground state concentrates around the origin. Figure 6(b) shows that the first $J^\pi = 1/2^-$ state of configurations $^{8}\text{Be} \otimes \Lambda[110]1/2^-$ gives a two-center distribution of Λ along the z axis corresponding to the $p^{\parallel}_{\Lambda}$ orbital. Figures 6(c) and 6(d) indicate that the first $J^\pi = 3/2^-$ and $J^\pi = 1/2^-$ states of the configurations $^{8}\text{Be} \otimes \Lambda[101]3/2^-$ and $^{8}\text{Be} \otimes \Lambda[101]1/2^-$ both give ring structures of the Λ distribution, and the former one is a little more diffused than the later one. Under the condition of rotational symmetry around the z axis, this kind of ring structure corresponds to the $p^{\perp}_{\Lambda}$ orbital.

In order to investigate the impurity effect of Λ hyperon on the nuclear core through $E2$ transition strength, the $B(E2)$ values of ^{8}Be, $^{9}_{\Lambda}$Be, and $^{10}_{\Lambda\Lambda}$Be are listed in Table I. In Ref. [70], the observed $B(E2,4^+_1 \to 2^+_1)$ of ^{8}Be is given as 21 ± 2.3 e^2 fm^4, while our calculated $B(E2)$ values for $2^+_1 \to 0^+_1$ and $4^+_1 \to 2^+_1$ are 21.97 and 32.88 e^2fm^4, respectively, which indicates that our model overestimates the $E2$ transition strength to some extent. Taking into consideration the fact that the beyond RMF model gives $B(E2,4^+_1 \to 2^+_1)$ as 47.28 e^2 fm^4 [51] and the microscopic cluster model calculations give it as 39.3 [8] or 30.0 e^2fm^4 [71], the results in the present work is acceptable.

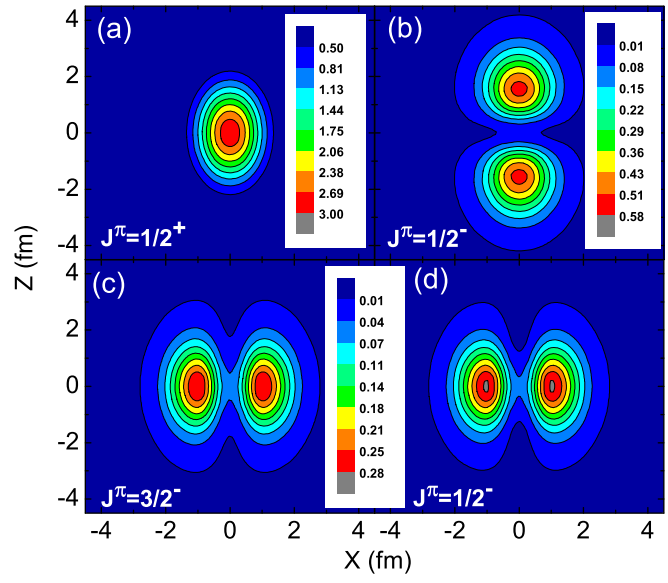

FIG. 6. Density distributions of Λ hyperon for the band heads of $^{9}_{\Lambda}$Be with configurations $^{8}\text{Be} \otimes \Lambda[000]1/2^+$ [panel (a)], $^{8}\text{Be} \otimes \Lambda[110]1/2^-$ [panel (b)], $^{8}\text{Be} \otimes \Lambda[101]3/2^-$ [panel (c)], and $^{8}\text{Be} \otimes \Lambda[101]1/2^-$ [panel (d)], respectively. Panels (c) and (d) share the same color bar. The unit is set as 10^{-2} fm^{-3} uniformly.

TABLE I. $E2$ transition strength for ^{8}Be, $^{9}_{\Lambda}$Be, and $^{10}_{\Lambda\Lambda}$Be and $cB(E2)$ values for the nuclear core in $^{9}_{\Lambda}$Be. The columns labeled by $cB(E2)^{*}$ represent the corresponding values of $B(E2,L \to L')$ taken from Ref. [8], and $B(E2)^{\dagger}$ and $cB(E2)^{\dagger}$ give the results obtained by PRM in Ref. [51]. The observed datum labeled by exp comes from Ref. [70].

^{8}Be				$^{9}_{\Lambda}$Be					$^{10}_{\Lambda\Lambda}$Be	
$J_i^{\pi} \to J_f^{\pi}$	$B(E2)$	$B(E2)^{*}$	$B(E2)^{\dagger}$	$J_i^{\pi} \to J_f^{\pi}$	$B(E2)$	$cB(E2)$	$cB(E2)^{*}$	$cB(E2)^{\dagger}$	$J_i^{\pi} \to J_f^{\pi}$	$B(E2)$
$2_1^+ \to 0_1^+$	21.97	22.4	24.99	$3/2_1^+ \to 1/2_1^+$	17.18	17.18	11.3	22.55	$2_1^+ \to 0_1^+$	13.86
				$5/2_1^+ \to 1/2_1^+$	17.20	17.20		22.57		
$4_1^+ \to 2_1^+$	32.88	39.3	47.28	$7/2_1^+ \to 3/2_1^+$	22.21	24.67	13.5	41.58	$4_1^+ \to 2_1^+$	18.66
exp:	21 ± 2.3			$9/2_1^+ \to 5/2_1^+$	24.36	24.36		41.55		
				$7/2_1^+ \to 5/2_1^+$	25.99	25.99		41.52		
				$5/2_1^- \to 1/2_1^-$	29.02	37.32	26.5	16.90		
				$7/2_1^- \to 3/2_1^-$	36.81	36.81		17.15		

In Ref. [8], to eliminate the trivial factor of $B(E2)$ caused by the angular momentum coupling for spin 1/2 of the Λ hyperon, the core transition rate is introduced for $^{9}_{\Lambda}$Be,

$$cB(E2,L_i \to L_f)_H \equiv \frac{1}{(2L_i+1)(2J_f+1)} \begin{Bmatrix} L_f & J_f & j_L \\ J_i & L_i & 2 \end{Bmatrix}^{-2} \times B(E2,J_i \to J_f), \quad (15)$$

where L_i and L_f are the initial and final angular momenta of the nuclear core and $j_L = 1/2$ for Λ. Using the core transition rate in $^{7}_{\Lambda}$Li, Refs. [8,21] successfully predict the size shrinkage effect, which is later confirmed in the experiment for the first time [72]. In this current paper, the core transition rates $cB(E2)$ are given in Table I and compared to the value taken from microscopic cluster model calculations [8] and PRM calculations [51]. We can see that $cB(E2,2_1^+ \to 0_1^+)$ for the positive-parity levels generated by the configuration $^{8}\text{Be} \otimes \Lambda[000]1/2^+$ is more than 20% smaller than $B(E2,2_1^+ \to 0_1^+)$ of ^{8}Be, which shows clearly the shrinkage effect of Λ occupying the s_Λ orbital. Compared to our results, the PRM calculations give less obvious shrinkage effect, while the microscopic cluster model calculations give a much more obvious one.

For $B(E2,5/2_1^- \to 1/2_1^-)$ and $B(E2,7/2_1^- \to 3/2_1^-)$, the corresponding $cB(E2)$ values are about 37 $e^2\,fm^4$, which are obviously larger than the ones given by the PRM and the microscopic cluster calculations. This contradiction may originate from the fact that the current calculation is a single-channel calculation, while the calculations in Ref. [51] are multichannel ones. Figure 6(b) shows that the orbital $\Lambda[110]1/2^-$ is prolately distributed and the two-α structure of the nuclear core is stretched by the Λ hyperon. Mixing with the oblately distributed orbitals such as $\Lambda[101]3/2^-$ and $\Lambda[101]1/2^-$ may reduce the weights of prolate configurations and make $cB(E2)$ values smaller.

IV. CONCLUSIONS

In this paper, properties of ^{8}Be, $^{9}_{\Lambda}$Be, and $^{10}_{\Lambda\Lambda}$Be are investigated by the beyond-mean-field SHF model with the SLy4+SLL4 interactions. The two-α structure are reproduced for the ground-band states of ^{8}Be. Through the comparison with the observed data and with the results of other models, it is shown that the calculated energy spectra and $E2$ transition strength are reasonable. The addition of a Λ hyperon to $\Lambda[000]1/2^+$ gives reasonable reproduction of the positive-parity energy levels compared to the experimental ones of $^{9}_{\Lambda}$Be, and the shrinkage effect makes the $E2$ transition strength reduced obviously. The Λ binding energy is 7.29 MeV which is about 0.5 MeV larger than the experimental data but much better than the result given by spherical configuration in Ref. [45]. The Λ hyperon occupying $\Lambda[110]1/2^-$ gives two spin doublets $(3/2^-,1/2^-)$ and $(7/2^-,5/2^-)$ which may be associated to the observed levels at 5.80 and 9.52 MeV, respectively, and these corresponds to the genuine hypernuclear states. This negative-parity configuration gives enhanced $E2$ transition strength due to its prolate density distribution. The other two negative-parity configurations, $^{8}\text{Be} \otimes \Lambda[101]3/2^-$ and $^{8}\text{Be} \otimes \Lambda[101]1/2^-$, reproduce the ^{9}Be-analog states near 12–13 MeV which are consistent with the observed data (the second peak of ^{9}Be (K^- in-flight, π^-) reaction [5]). The double-Λ hypernucleus, $^{10}_{\Lambda\Lambda}$Be, is also investigated as a test of the current model with two Λ's occupying $\Lambda[000]1/2^+$ and its time-reversal partner, and the double-Λ binding energy is overestimated to some extent if the attractive $\Lambda\Lambda$ interaction $\langle V_{\Lambda\Lambda}\rangle$ is taken into account as a correction.

Finally, we can conclude that the beyond-mean-field SHF model with the SLL4 $N\Lambda$ interaction is reasonable and effective to describe the energy spectrum of $^{9}_{\Lambda}$Be with a three-body cluster structure, although it slightly overestimates the Λ binding energy.

ACKNOWLEDGMENTS

The authors thank H.-J. Schulze and S.-G. Zhou for informative discussions. This work was supported by the National Natural Science Foundation of China (Grant No. 11775081, and No. 11547044) and Natural Science Foundation of Shanghai (Grant No. 17ZR1408900), and Open Project Program of State Key Laboratory of Theoretical Physics, Institute of Theoretical Physics, Chinese Academy of Sciences, China (Grant No.Y5KF141CJ1).

[1] D. H. Davis, Nucl. Phys. A **754**, 3c (2005).
[2] O. Hashimoto and H. Tamura, Prog. Part. and Nucl. Phys. **57**, 564 (2006).
[3] E. Botta, T. Bressani, and G. Garbarino, Eur. Phys. J. A **48**, 41 (2012).
[4] A. Gal, E. V. Hungerford, and D. J. Millener, Rev. Mod. Phys. **88**, 035004 (2016).
[5] W. Brückner, M. A. Faessler, K. Kilian, U. Lynen, B. Pietrzyk, B. Povh, H. G. Ritter, B. Schürlein, H. Schröder, and A. H. Walenta, Phys. Lett. B **55**, 107 (1975); W. Brückner, B. Granz, D. Ingham, K. Kilian, U. Lynen, J. Niewisch, B. Pietrzyk, B. Povh, H. G. Ritter, and H. Schröder, *ibid.* **62**, 481 (1976); W. Brückner, M. A. Faessler, T. J. Ketel, K. Kilian, J. Niewischab, B. Povhab, H. G. Ritterab, M. Uhrmacherab, P. Birienc, H. Catzc *et al.*, *ibid.* **79**, 157 (1978).
[6] R. H. Dalitz and A. Gal, Phys. Rev. Lett. **36**, 362 (1976).
[7] H. Bando, M. Seki, and Y. Shono, Prog. Theor. Phys. **66**, 2118 (1981).
[8] T. Motoba, H. Bando, and K. Ikeda, Prog. Theor. Phys. **70**, 189 (1983).
[9] T. Motoba, H. Bando, and K. Ikeda, Prog. Theor. Phys. **71**, 222 (1984).
[10] E. H Auerbach, A. J. Baltz, C. B. Dover, A. Gal, S. H. Kahana, L. Ludeking, and D. J. Millener, Ann. Phys. **148**, 381 (1983).
[11] H. Bando, Nucl. Phys. A **450**, 217c (1986).
[12] T. Yamada, K. Ikeda, H. Bando, and T. Motoba, Phys. Rev. C **38**, 854 (1988).
[13] P. H. Pile, S. Bart, R. E. Chrien, D. J. Millener, R. J. Sutter, N. Tsoupas, J.-C. Peng, C. S. Mishra, E. V. Hungerford, T. Kishimoto *et al.*, Phys. Rev. Lett. **66**, 2585 (1991).
[14] S. Ajimura, K. Aoki, H. Bhang, T. Endo, Y. Fujii, O. Hashimoto, H. Hotchi, E. Hungerford, J. H. Kim, Y. D. Kim *et al.*, Nucl. Phys. A **639**, 93c (1998).
[15] J. K. Ahn, Y. Akaishi, H. Akikawa, S. Aoki, K. Arai, Y. S. Bahk, M. K. Baik, B. Bassalleck, H. J. Chung, S. M. Chung *et al.*, *Hadrons and Nuclei*, AIP Conf. Proc. 594 (AIP, New York, 2001), p. 180.
[16] E. Hiyama, M. Kamimura, T. Motoba, T. Yamada, and Y. Yamamoto, Phys. Rev. C **66**, 024007 (2002).
[17] A. Gal and D. J. Millener, Phys. Lett. B **701**, 342 (2011).
[18] A. Gal, J. M. Soper, and R. H. Dalitz, Ann. Phys. (NY) **63**, 53 (1971).
[19] A. Gal, J. M. Soper, and R. H. Dalitz, Ann. Phys. (NY) **72**, 455 (1972).
[20] A. Gal, Nucl. Phys. A **754**, 91c (2005).
[21] E. Hiyama, M. Kamimura, K. Miyazaki, and T. Motoba, Phys. Rev. C **59**, 2351 (1999).
[22] E. Hiyama, M. Kamimura, T. Motoba, T. Yamada, and Y. Yamamoto, Phys. Rev. Lett. **85**, 270 (2000).
[23] E. Hiyama, Y. Yamamoto, T. Motoba, and M. Kamimura, Phys. Rev. C **80**, 054321 (2009).
[24] E. Hiyama, M. Kamimura, Y. Yamamoto, and T. Motoba, Phys. Rev. Lett. **104**, 212502 (2010).
[25] M. Rayet, Nucl. Phys. A **367**, 381 (1981).
[26] J. Cugnon, A. Lejeune, and H.-J. Schulze, Phys. Rev. C **62**, 064308 (2000).
[27] I. Vidaña, A. Polls, A. Ramos, and H.-J. Schulze, Phys. Rev. C **64**, 044301 (2001).
[28] X.-R. Zhou, H.-J. Schulze, H. Sagawa, C.-X. Wu, and E.-G. Zhao, Phys. Rev. C **76**, 034312 (2007).
[29] X.-R. Zhou, A. Polls, H.-J. Schulze, and I. Vidaña, Phys. Rev. C **78**, 054306 (2008).
[30] M.-T. Win, K. Hagino, and T. Koike, Phys. Rev. C **83**, 014301 (2011).
[31] H.-J. Schulze and T. Rijken, Phys. Rev. C **88**, 024322 (2013).
[32] X.-R. Zhou, E. Hiyama, and H. Sagawa, Phys. Rev. C **94**, 024331 (2016).
[33] M.-T. Win and K. Hagino, Phys. Rev. C **78**, 054311 (2008).
[34] C. Y. Song, J. M Yao, H. F. Lü, and J. Meng, Int. J. Mod. Phys. E **19**, 2538 (2010).
[35] B.-N. Lu, E.-G. Zhao, and S.-G. Zhou, Phys. Rev. C **84**, 014328 (2011).
[36] Y. Tanimura and K. Hagino, Phys. Rev. C **85**, 014306 (2012).
[37] B.-N. Lu, E. Hiyama, H. Sagawa, and S.-G. Zhou, Phys. Rev. C **89**, 044307 (2014).
[38] R. L. Xu, C. Wu, and Z. Z. Ren, Nucl. Phys. A **933**, 82 (2015).
[39] Y. Kanada-En'yo, H. Horiuchi, and A. Ono, Phys. Rev. C **52**, 628 (1995).
[40] M. Isaka, M. Kimura, A. Dote, and A. Ohnishi, Phys. Rev. C **83**, 044323 (2011); **83**, 054304 (2011).
[41] M. Isaka, H. Homma, M. Kimura, A. Dote, and A. Ohnishi, Phys. Rev. C **85**, 034303 (2012).
[42] M. Isaka, M. Kimura, A. Dote, and A. Ohnishi, Phys. Rev. C **87**, 021304(R) (2013).
[43] M. Isaka and M. Kimura, Phys. Rev. C **92**, 044326 (2015).
[44] R. Wirth, D. Gazda, P. Navratil, A. Calci, J. Langhammer, and R. Roth, Phys. Rev. Lett. **113**, 192502 (2014).
[45] H.-J. Schulze and E. Hiyama, Phys. Rev. C **90**, 047301 (2014).
[46] H. Mei, K. Hagino, and J. M. Yao, Phys. Rev. C **93**, 011301(R) (2016).
[47] X. Y. Wu, H. Mei, J. M. Yao, and X.-R. Zhou, Phys. Rev. C **95**, 034309 (2017).
[48] J.-W. Cui, X.-R. Zhou, L.-X. Guo, and H.-J. Schulze, Phys. Rev. C **95**, 024323 (2017).
[49] J.-W. Cui and X.-R. Zhou, Prog. Theor. Exp. Phys. **2017**, 093D04 (2017).
[50] J. M. Yao, Z. P. Li, K. Hagino, M.-T. Win, Y. Zhang, and J. Meng, Nucl. Phys. A **868**, 12 (2011).
[51] H. Mei, K. Hagino, J. M. Yao, and T. Motoba, Phys. Rev. C **90**, 064302 (2014).
[52] W. X. Xue, J. M. Yao, K. Hagino, Z. P. Li, H. Mei, and Y. Tanimura, Phys. Rev. C **91**, 024327 (2015).
[53] H. Mei, K. Hagino, J. M. Yao, and T. Motoba, Phys. Rev. C **91**, 064305 (2015).
[54] H. Mei, K. Hagino, J. M. Yao, and T. Motoba, Phys. Rev. C **93**, 044307 (2016).
[55] M. Bender, K. Rutz, P.-G. Reinhard, and J. A. Maruhn, Eur. Phys. J. A **8**, 59 (2000).
[56] P. Ring and P. Schuck, *The Nuclear Many-Body Problem* (Springer, Berlin, 1980).
[57] R. Rodriguez-Guzman, J. L. Egido, and L. M. Robledo, Phys. Lett. B **474**, 15 (2000).
[58] P. Bonche, J. Dobaczewski, H. Flocard, P.-H. Heenen, and J. Meyer, Nucl. Phys. A **510**, 466 (1990).
[59] J. M. Yao, H. Mei, H. Chen, J. Meng, P. Ring, and D. Vretenar, Phys. Rev. C **83**, 014308 (2011).
[60] J. Dobaczewski, W. Satuła, B. G. Carlsson, J. Engel, P. Olbratowski, P. Powałowski, M. Sadziak, J. Sarich, N. Schunck, A. Staszczak *et al.*, Comput. Phys. Commun. **180**, 2361 (2009).
[61] H. Sagawa, X.-R. Zhou, X.-Z. Zhang, and T. Suzuki, Phys. Rev. C **70**, 054316 (2004).

[62] J. Terasaki, P.-H. Heenen, H. Flocard, and P. Bonche, Nucl. Phys. A **600**, 371 (1996).
[63] J.-W. Cui, X.-R. Zhou, and H.-J. Schulze, Phys. Rev. C **91**, 054306 (2015).
[64] H. Kohri, S. Ajimura, H. Hayakawa, T. Kishimoto, K. Matsuoka, S. Minami, Y. S. Miyake, T. Mori, K. Morikubo, E. Saji *et al.*, Phys. Rev. C **65**, 034607 (2002).
[65] W. Greiner and J. A. Maruhn, *Nuclear Models* (Springer-Verlag, Berlin, 1996).
[66] National Nuclear Data Center [http://www.nndc.bnl.gov/].
[67] M. Jurič, G. Bohm, J. Klabuhn, U. Krecker, F. Wysotzki, G. Coremans-Bertrand, J. Sacton, G. Wilquet, T. Cantwell, F. Esmael *et al.*, Nucl. Phys. B **52**, 1 (1973).
[68] H. Tamura, S. Ajimura, H. Akikawa, D. E. Alburger, K. Aoki, A. Banu, R. E. Chrien, G. B. Franklin, J. Franz, Y. Fujii *et al.*, Nucl. Phys. A **754**, 58c (2005).
[69] H. Akikawa, S. Ajimura, R. E. Chrien, P. M. Eugenio, G. B. Franklin, J. Franz, L. Gang, K. Imai, P. Khaustov, M. May *et al.*, Phys. Rev. Lett. **88**, 082501 (2002).
[70] V. M. Datar, D. R. Chakrabarty, S. Kumar, V. Nanal, S. Pastore, R. B. Wiringa, S. P. Behera, A. Chatterjee, D. Jenkins, C. J. Lister *et al.*, Phys. Rev. Lett. **111**, 062502 (2013).
[71] Y. You-wen, T. Motoba, and H. Bandō, Prog. Theor. Phys. **76**, 861 (1986).
[72] K. Tanida, H. Tamura, D. Abe, H. Akikawa, K. Araki, H. Bhang, T. Endo, Y. Fujii, T. Fukuda, O. Hashimoto *et al.*, Phys. Rev. Lett. **86**, 1982 (2001).